

---

# Output Model-Following Control Synthesis for an Oblique-Wing Aircraft

---

Joseph W. Pahle

---

April 1990

---

# Output Model-Following Control Synthesis for an Oblique-Wing Aircraft

---

Joseph W. Pahle  
Ames Research Center, Dryden Flight Research Facility, Edwards, California

1990



National Aeronautics and  
Space Administration

Ames Research Center

Dryden Flight Research Facility  
Edwards, California 93523-0273

**CONTENTS**

**SUMMARY** 1

**NOMENCLATURE** 1

    Subscripts . . . . . 2

    Superscripts . . . . . 2

**INTRODUCTION** 2

**PROBLEM DEFINITION** 3

**OUTPUT ERROR LINEAR QUADRATIC REGULATOR** 3

**OBLIQUE WING RESEARCH AIRCRAFT DESCRIPTION** 6

**OBLIQUE WING RESEARCH AIRCRAFT DESIGN EXAMPLE** 7

**RESULTS** 8

**APPENDIX** 12

**REFERENCES** 14

## SUMMARY

A decoupling control law synthesis technique is presented that integrates stability augmentation, decoupling, and the direct incorporation of desired handling qualities into an output feedback controller. The proposed design technique uses linear quadratic regulator (LQR) concepts in the framework of explicit model following (EMF) and proportional plus integral (PI) feedback. An idealized model is used as a part of the controller for robustness and handling qualities requirements. The PI error feedback is used to balance model-following performance with surface activity and to force steady-state errors to zero. The output feedback gains are then computed from a projection of the full-state gains. Closed-loop performance is shown by application of the control laws to the linearized equations of motion, and a six-degree-of-freedom simulation of an oblique-wing aircraft. Model following is shown to be quite good, but with some significant time delay in both linear and nonlinear evaluations. Decoupling of the longitudinal and lateral-directional axes is excellent, with some small oscillations evident in the nonlinear responses.

## NOMENCLATURE

$A, B, H, F$	state space quadruple defining the model state and output equations
$a_n$	normal acceleration, $g$
$a_y$	lateral acceleration, $g$
$C$	error selection matrix
DFBW	digital fly by wire
EMF	explicit model following
$I_n$	identity matrix of dimension $n$
$i$	$\sqrt{-1}$
$J$	quadratic cost function
$K_x$	state feedback gain matrix
$K_y$	output feedback gain matrix
LQR	linear quadratic regulator
$M$	Mach number
OWRA	oblique wing research aircraft
PI	proportional plus integral
$p$	roll rate, deg/sec
$Q$	quadratic state weighting matrix
$q$	pitch rate, deg/sec
$R$	quadratic control input weighting matrix
$r$	yaw rate, deg/sec
$S$	quadratic cross-weighting matrix for states and inputs
$u$	control vector
$W$	output vector weighting matrix
$x$	state vector

$y$	output vector
$y_e$	output error vector
$\alpha$	angle of attack, deg
$\beta$	angle of sideslip, deg
$\delta_{aL}$	left aileron deflection, deg
$\delta_{aR}$	right aileron deflection, deg
$\delta_{hL}$	left horizontal tail deflection, deg
$\delta_{hR}$	right horizontal tail deflection, deg
$\delta_R$	rudder deflection, deg
$\phi$	roll angle, deg

### Subscripts

$e$	error
$Ie$	integral error
$m$	model
$p$	plant

### Superscripts

T	complex conjugate transpose
---	-----------------------------

## INTRODUCTION

Early wind-tunnel and theoretical studies have shown that a variable-skew oblique wing offers a substantial aerodynamic advantage over conventional or symmetric variable-sweep aircraft for missions that require both subsonic loiter and supersonic dash or cruise (Nelms, 1976 and Wiler, 1985). The NASA Ames Research Center, Dryden Flight Research Facility AD-1 flight program successfully demonstrated the oblique-wing concept and explored the low subsonic handling qualities and performance envelope (McMurtry, 1981). Because most of the aerodynamic advantage occurs at transonic and supersonic speeds, a high-speed flight research program was jointly sponsored by Ames-Dryden and the U.S. Navy. The oblique wing research aircraft (OWRA) was to be based on a modified F-8 digital fly-by-wire (DFBW) aircraft with a composite wing and wing-pivot mechanism substituted for the existing high wing structure (fig. 1).

A major challenge in the OWRA program is the design and implementation of a control system architecture that will provide stabilization, decoupling, and acceptable flying qualities across the Mach number ( $M$ ), angle-of-attack, and wing-skew envelope. Because of the vehicle dynamic cross-coupling, the control system design must be applied to at least five (rigid body) degrees of freedom simultaneously, rather than separating the problem into the more typical two or three degrees of freedom in the longitudinal- and lateral-directional modes. The OWRA configuration provides an excellent opportunity to apply modern control methodologies to the problems associated with an oblique-wing configuration.

Model following has been shown to be an effective method for decoupling and stabilization of an initial OWRA configuration in previous work by Alag and others (1986). Implicit and explicit model-following (EMF) techniques were used successfully in a variety of controller structures to decouple the aircraft dynamics, but control surface activity was normally high, and steady-state model-following errors degraded the control system performance over a period of time.

Vincent (1984) proposed an integrated model-following technique where dynamic elements are introduced into the constant gain controller to reduce steady-state model-following errors, and a nonoptimal output-feedback strategy is used to implement the resulting control law in a realizable form. In this way, handling quality requirements and trajectory tracking can be directly incorporated into a linear quadratic regulator (LQR) synthesis technique. Output error weighting is used instead of state weighting in the LQR cost functional, which gives the designer a better physical feel for the parameters being minimized.

This paper presents a form of the integrated model-following technique as applied to the OWRA model. The resulting controller is structured as a proportional plus integral (PI) output-feedback control law. The effectiveness of the controller is shown by closed-loop time responses from linearized equations of motion as well as nonlinear six-degree-of-freedom simulation results at a given high subsonic flight condition and wing-skew position.

## PROBLEM DEFINITION

Model-following is a useful technique when the dynamic characteristics for an ideal model can be specified. In EMF, the dynamic model is an integral part of the controller itself. The objective of EMF control is to force the aircraft to respond as the model would to a given pilot command. The model-following problem can be stated as follows:

Given the linearized plant dynamic equation

$$\dot{\mathbf{x}}_p = A_p \mathbf{x}_p + B_p \mathbf{u}_p \quad (1)$$

and the linearized model dynamics

$$\dot{\mathbf{x}}_m = A_m \mathbf{x}_m + B_m \mathbf{u}_m \quad (2)$$

where  $\mathbf{x}_p$ ,  $\mathbf{x}_m$ ,  $\mathbf{u}_p$ , and  $\mathbf{u}_m$  are real vectors, and all matrices  $A_p$ ,  $A_m$ ,  $B_p$ , and  $B_m$  are of suitable dimensions, find the control  $\mathbf{u}_p$  that will force the aircraft states  $\mathbf{x}_p$  to approximate the model states  $\mathbf{x}_m$ . Although sufficient conditions exist for guaranteeing "exact" or perfect model following, the conditions cannot be met by a physical system (Tyler, 1964). This problem definition can be put in the context of the LQR, where the cost functional can be expressed in terms of the plant and model states or outputs. Therefore, the squared error between the plant and the model would be minimized, forcing the plant to follow the model states or outputs. An output error LQR formulation was used in this investigation primarily to simplify the task of selecting cost function weighting matrices and to give the designer better insight into the parameters being minimized.

## OUTPUT ERROR LINEAR QUADRATIC REGULATOR

Consider the aircraft plant and model dynamic equations given above in equations (1), (2), and the output equations

$$\mathbf{y}_p = H_p \mathbf{x}_p + F_p \mathbf{u}_p \quad (3)$$

$$\mathbf{y}_m = H_m \mathbf{x}_m + F_m \mathbf{u}_m \quad (4)$$

The most common form of the quadratic cost is a function of the state and control vectors of the system, written as

$$J = \int_0^{\infty} \mathbf{x}^T Q \mathbf{x} + \mathbf{u}^T R \mathbf{u} dt \quad (5)$$

or in output formulation

$$J = \int_0^{\infty} \mathbf{y}^T Q \mathbf{y} + \mathbf{u}^T R \mathbf{u} dt \quad (6)$$

where  $Q > 0$  and  $R \geq 0$  are the quadratic weighting matrices. Define the output error as  $\mathbf{y}_e = \mathbf{y}_p - \mathbf{y}_m$  to determine the cost as a function of the error between the plant and model outputs. Integral error can be added by defining the error state equation:

$$\dot{\mathbf{x}}_{Ie} = C \mathbf{y}_e \quad (7)$$

where  $C$  is a selection matrix operating on the output error vector. Thus the state and output equations can be augmented to form the following system:

$$\underbrace{\begin{bmatrix} \dot{\mathbf{x}}_p \\ \dot{\mathbf{x}}_{Ie} \\ \dot{\mathbf{x}}_m \end{bmatrix}}_{\dot{\mathbf{x}}} = \underbrace{\begin{bmatrix} A_p & 0 & 0 \\ CH_p & 0 & -CH_m \\ 0 & 0 & A_m \end{bmatrix}}_A \underbrace{\begin{bmatrix} \mathbf{x}_p \\ \mathbf{x}_{Ie} \\ \mathbf{x}_m \end{bmatrix}}_{\mathbf{x}} + \underbrace{\begin{bmatrix} B_p & 0 \\ CF_p & -CF_m \\ 0 & B_m \end{bmatrix}}_B \underbrace{\begin{bmatrix} \mathbf{u}_p \\ \mathbf{u}_m \end{bmatrix}}_{\mathbf{u}} \quad (8)$$

$$\mathbf{y} = \begin{bmatrix} \mathbf{y}_e \\ \mathbf{y}_{Ie} \\ \mathbf{y}_m \end{bmatrix} = \underbrace{\begin{bmatrix} H_p & 0 & -H_m \\ 0 & I & 0 \\ 0 & 0 & H_m \end{bmatrix}}_H \underbrace{\begin{bmatrix} \mathbf{x}_p \\ \mathbf{x}_{Ie} \\ \mathbf{x}_m \end{bmatrix}}_{\mathbf{x}} + \underbrace{\begin{bmatrix} F_p & -F_m \\ 0 & 0 \\ 0 & F_m \end{bmatrix}}_F \underbrace{\begin{bmatrix} \mathbf{u}_p \\ \mathbf{u}_m \end{bmatrix}}_{\mathbf{u}} \quad (9)$$

Since the output equation (9) is a linear function of the states and controls, the cost functional equation (6) can then be restated as

$$J = \int_0^{\infty} \mathbf{x}^T \tilde{Q} \mathbf{x} + \mathbf{x}^T \tilde{S} \mathbf{u} + \mathbf{u}^T \tilde{S}^T \mathbf{x} + \mathbf{u}^T \tilde{R} \mathbf{u} dt \quad (10)$$

with  $\tilde{Q} > 0$  and  $\tilde{R} \geq 0$ ,  $\tilde{S} \geq 0$ , and given by

$$\tilde{Q} = \begin{bmatrix} H_p^T Q_e H_p & 0 & -H_p^T Q_e H_m \\ 0 & Q_{Ie} & 0 \\ -H_m^T Q_e H_p & 0 & H_m^T Q_e H_m \end{bmatrix} \quad (11)$$

$$\tilde{S} = \begin{bmatrix} H_p^T Q_e F_p & -H_p^T Q_e F_m \\ 0 & 0 \\ -H_m^T Q_e F_p & H_m^T Q_e F_m \end{bmatrix} \quad (12)$$

$$\tilde{R} = \begin{bmatrix} F_p^T Q_e F_p & -F_p^T Q_e F_m \\ -F_m^T Q_e F_p & F_m^T Q_e F_m \end{bmatrix} + R \quad (13)$$

where  $Q_e$  is the weighting matrix for the output error terms, and  $Q_{Ie}$  is the weighting matrix for the integral error terms. If  $(A, B)$  is stabilizable, and  $(H, A)$  is observable, the linear steady-state optimal control that minimizes  $J$  equation (10) is found by solving the steady-state Riccati equation (Bryson, 1975), and is of the form

$$\mathbf{u} = -K_x \mathbf{x} \quad (14)$$

The resulting optimal control law is a function of all the states in the augmented system. A projection from the state space to the output space is possible without changing the closed-loop eigenvalues (appendix) if the number of unique outputs is equal to or greater than the number of states in the augmented system. The resulting eigenvectors are not guaranteed to be unchanged, but the model-following control structure will dominate the response behavior by driving the error and integral error to zero. This projection can be stated as follows:

Define a weighted output vector

$$\bar{y} = W y = \bar{H} x + \bar{F} u$$

where  $\bar{H} = W H$ , and  $\bar{F} = W F$ .

Since  $\bar{H}$  is assumed full rank, and  $(\bar{H}^T \bar{H}) > 0$ , this implies that  $(\bar{H}^T \bar{H})^{-1}$  exists. The output equation can then be rewritten in terms of the system states as

$$x = (\bar{H}^T \bar{H})^{-1} \bar{H}^T \bar{y} - (\bar{H}^T \bar{H})^{-1} \bar{H}^T \bar{F} u \quad (15)$$

The optimal control can therefore be written in the output form

$$u = - \underbrace{[I - K_x (\bar{H}^T \bar{H})^{-1} \bar{H}^T \bar{F}]^{-1} K_x (\bar{H}^T \bar{H})^{-1} \bar{H}^T}_{K_y} \bar{y} \quad (16)$$

where  $K_y$  can be partitioned as  $[K_p K_{Ie} K_m]$  (see fig. 2).

It can be shown that if  $\bar{y} = x$  (this implies  $H = W = I$  and  $F = 0$ ), it is possible to reduce the above equation to the state form of the optimal control law equation (14).  $W$  and  $R$  can be chosen in such a way that only the desired output feedback paths will have nontrivial gain values. Thus, all the feedback loops to the model can be eliminated, preserving the desired closed-loop eigenvalues of the idealized model. The control system design procedure can be stated as follows:

1. Determine idealized model dynamics,
2. Choose quadratic cost matrices  $Q_e, R, Q_{Ie}$ ,
3. Calculate optimal state feedback gains  $K_x$  from steady-state Riccati equation,
4. Choose output weighting matrix  $W$  so that only the desired feedback loops have nontrivial gains,
5. Determine output feedback gains  $K_y$  from state gain projection, and
6. Iterate steps two through five until desired system performance is achieved.

Figure 2 shows a block diagram of the final PI feedback controller. The resulting control law is nonoptimal in a strict sense because of the gain projection, but the design technique incorporates some important features.

1. The output error formulation allows the designer to balance model-following performance with control surface activity, both in surface deflection and rate (if the actuator dynamics are modeled in the plant),
2. The integral error feedback forces steady-state model-following errors to zero, thus making the control law more robust to modeling errors in the aircraft plant dynamics,
3. The idealized dynamic feedforward model allows the incorporation of lead-lag networks, stick prefilters, or general command shaping in the forward loop for handling qualities requirements, and

4. The augmented control system structure, a dynamic prefilter with PI error feedback, is similar to classical PI controllers. Therefore, designers can apply knowledge and intuition from past design experience, an important factor in a highly interrelated problem.

As in most methodologies, this synthesis technique has some drawbacks.

1. The number of resulting gains, even in the output error formulation, is prohibitively high, and gain scheduling between flight conditions is a complex problem.
2. Although the full state LQR has guaranteed phase and gain margins, the projection from state to output space negates any robustness guarantees except for closed-loop stability.
3. The selection of the proper weighting matrices  $Q_e$  and  $R$  is not a straightforward process. This problem is made more difficult because the desired time or frequency response behavior not specified in the model cannot be easily related to the weighting matrices. Additionally, great care must be taken when implementing a linear idealized model (perturbation model, valid only for small angle maneuvers, instantaneous response to inputs, etc.) in a nonlinear, six-degree-of-freedom flight system.

It is hoped that future research can overcome these drawbacks and allow this technique to be applied to a broader class of problems.

## OBLIQUE WING RESEARCH AIRCRAFT DESCRIPTION

The F-8 OWRA design configuration was based on a feasibility design study done by Rockwell International (White and others, 1984) which had its roots in the initial work done at NASA Ames Research Center in the early 70s (Graham and others, 1985; Smith and others, 1975 and 1976). The F-8 OWRA is basically the F-8 DFBW aircraft with the 357 ft<sup>2</sup> wing replaced by a 200 ft<sup>2</sup> composite wing and pivot structure (fig. 1). Wing skew is right wing forward, from 0 (unskewed) to 65°.

The OWRA aerodynamic model was based on a combination of wind-tunnel studies, computational fluid dynamics, and the simulation aerodynamic database of the F-8 DFBW aircraft. Much of the data from all three sources had to be linearized, interpolated, or modified in some way to form a cohesive full-envelope aerodynamic model. This modified aerodynamic model was implemented in a six-degree-of-freedom, nonlinear, fixed-base simulation used for piloted evaluation and control systems development. Linear models used in the control system design were obtained from this nonlinear aerodynamic model using the program LINEAR (Duke, 1987). A comparison of linear and nonlinear open-loop time histories showed excellent agreement indicating that the linear models could be used even at the maximum wing-skew conditions.

The engine model for the F-8 OWRA is based on the simulation engine model of the F-8 DFBW. The engine is equipped with an afterburner and is modeled in the simulation as two main rotational elements (compressor and fan) co-located along the thrust line in the vehicle x-z plane.

Different types of trim exist because of the unique aerodynamics of oblique-wing configurations. Trim is defined as the conditions necessary to set the derivative of the state vector ( $\dot{\mathbf{x}}$ ) to zero. When the wing is skewed, a nonzero sideslip angle  $\beta$  or roll angle  $\phi$  is required to keep the trim  $\dot{\phi} = \dot{\beta} = 0$  simultaneously. For this reason, level trim is defined as wings level ( $\phi = 0$ ) varying  $\beta$  as trim requires, and sideslip trim is defined as constant  $\beta$  (nominally zero) varying  $\phi$  as required. Figure 3 shows the relationship between trim  $\beta$  and trim  $\phi$  at a single flight condition.

Although many potential trim strategies exist, the ailerons are used to trim the roll axis, symmetric horizontal tail is used to trim the pitch axis, rudder is used to trim the yaw axis, and the throttle is used to obtain a steady-state velocity. Inboard flaps are used for unskewed powered approach only. Each surface moves independently, allowing

the controls designer greater flexibility in surface management which becomes more important at the high skew conditions, where the ailerons are effective (but highly coupled) controllers in all three axes.

## OBLIQUE WING RESEARCH AIRCRAFT DESIGN EXAMPLE

The OWRA design problem is well suited to the EMF design technique because a realistic model exists with the desired time response characteristics and closed-loop eigenvalues. The model used was a six-state approximation to the closed-loop dynamics of the OWRA at zero wing skew (table 2). A simple rate and acceleration feedback control system was designed for the unskewed aerodynamics and then implemented in a six-degree-of-freedom fixed-base simulation. The feedback gains for this simple control system were modified until satisfactory pilot comments were obtained. Linear models were then generated to approximate the closed-loop performance of this augmented system. The six states used were the minimum number required to incorporate four of the five classical rigid-body dynamic modes: short period, dutch roll, spiral, and roll mode. It was not necessary to include the open-loop phugoid mode in the desired model dynamics because it remains stable and relatively fixed throughout most of the flight envelope. The use of the zero-skew aircraft as a model has an additional benefit because the desired closed-loop dynamics of the aircraft remained constant over the wing-skew envelope. Thus, the pilot would not have to adapt to new characteristics as the wing is skewed.

For the OWRA design example, the model and plant state vector is given by

$$\mathbf{x} = \begin{bmatrix} \alpha \\ \beta \\ \phi \\ p \\ q \\ r \end{bmatrix} \begin{array}{l} \text{angle of attack, rad} \\ \text{sideslip angle, rad} \\ \text{roll angle, rad} \\ \text{roll rate, rad/sec} \\ \text{pitch rate, rad/sec} \\ \text{yaw rate, rad/sec} \end{array} \quad (17)$$

and the control vector

$$\mathbf{u} = \begin{bmatrix} \delta_{hL} \\ \delta_{hR} \\ \delta_{aL} \\ \delta_{aR} \\ \delta_R \end{bmatrix} \begin{array}{l} \text{left horizontal tail deflection, rad} \\ \text{right horizontal tail deflection, rad} \\ \text{left aileron deflection, rad} \\ \text{right aileron deflection, rad} \\ \text{rudder deflection, rad} \end{array} \quad (18)$$

Actuators were not modeled to simplify the design process and to reduce the number of feedback gains required. Because of this, only surface deflection could be directly minimized in the design, as no cost was incurred because of the surface deflection rate. Numerical difficulties were encountered in the full-state feedback gain projection to output feedback when actuator dynamics were included in the augmented state vector. These difficulties were primarily a function of the limited number of output parameters that were selected for feedback, rather than a fundamental limitation of the technique. The output parameters chosen were those typically used as feedback signals in classical control systems, especially those parameters related to the lateral-directional axis. Signal reliability and sensor redundancy were also factors in the selection. The output vector was identical for the model and the plant. The output error  $\mathbf{y}_e$  is given below as

$$\mathbf{y}_e = \begin{bmatrix} p_e \\ q_e \\ r_e \\ \phi_e \\ a_{ne} \\ a_{ye} \end{bmatrix} \begin{array}{l} \text{roll rate error, rad/sec} \\ \text{pitch rate error, rad/sec} \\ \text{yaw rate error, rad/sec} \\ \text{roll angle error, rad} \\ \text{normal acceleration error, } g \\ \text{lateral acceleration error, } g \end{array} \quad (19)$$

with the error between the three angular rates of the plant and model

$$\dot{y}_{Ie} = \begin{bmatrix} p_e \\ q_e \\ r_e \end{bmatrix} \begin{array}{l} \text{roll rate error, rad/sec} \\ \text{pitch rate error, rad/sec} \\ \text{yaw rate error, rad/sec} \end{array} \quad (20)$$

used as the input to the integral error feedback  $y_{Ie}$ . The angular rates were chosen as integral error feedbacks to improve the steady-state model following and add additional damping to cross-axis perturbations.

## RESULTS

The design flight condition was  $M = 0.8$ , altitude = 20,000 ft, and wing skew = 45°. This flight condition was chosen because it was contained in the proposed initial flight test envelope, and the cross-axis coupling was near a worst case for the entire flight envelope. Additionally, the total aircraft drag was near a minimum at the 45° wing-skew condition (fig. 4). Tables 1 and 2 show the system matrices for the plant and model respectively.

Many design iterations were used to determine a set of weighting matrices that resulted in good system performance with low control surface activity. The final matrices used were the following:  $Q_e = \text{DIAG}([10, 20, 10, 500, 10, 100])$ ,  $Q_{Ie} = \text{DIAG}([500, 500, 100])$ , and  $R = \text{DIAG}([200 I_5; 10^7 I_5])$ . The large values in  $R$  are applied to  $u_m$  to eliminate any feedback loops to the model. The output weighting matrix  $W$  was constructed to eliminate all but the desired feedback gains. In this case,  $W = \text{DIAG}([I_9; 10^{-5} I_6])$ . The resulting output feedback gain matrices  $K_p, K_{Ie}, K_m$  are shown in table 4. For this design case, it is interesting to note that the number of unique outputs is less than the number of states ( $\text{Rank}(H) = 9, \text{Rank}(A) = 15$ ), yet the eigenvalues for the output feedback system remain close to the eigenvalues of the full-state system (table 3).

The responses of the linearized open-loop aircraft model to a 1°-ramp in elevator and aileron are shown in figures 5–6. The ramp begins at 1 sec and ends at 3 sec for each input. The open-loop aircraft responses are lightly damped (note  $\alpha, q$ , and the accelerations) and the roll angle ( $\phi$ ) due to pitch command is larger in magnitude than the roll angle due to roll command. The roll response in the pitch axis was found to be a strong function of angle of attack as well as nonlinear at this flight condition. For this reason, only small amplitude inputs were used in the design evaluations, since the linear models were not valid for large amplitude maneuvers. Time histories for the closed-loop system were run initially with linear aerodynamics and nonlinear actuator models with rate and surface limits included.

After some design iterations, the control laws were implemented and tested in the nonlinear six-degree-of-freedom simulation. Figures 7–14 show the ideal linear model and closed-loop aircraft responses (both linear and nonlinear) to a 4°-roll ramp, while figures 15–22 show the responses to a 5°-pitch ramp. The closed-loop system is much more damped, and the roll due to pitch command has been all but eliminated. Good model following is evident, but with some significant time delay evident for both linear and nonlinear cases; note  $\phi$  and lateral acceleration for the roll input, and  $q, \alpha$ , for the pitch input. Oscillations can be seen in the nonlinear responses, especially in the cross-axis components, but the amplitudes are quite small.

*Ames Research Center  
Dryden Flight Research Facility  
National Aeronautics and Space Administration  
Edwards, California, October 6, 1989*

Table 1. Open-loop system matrices flight condition;  $M = 0.8$ , altitude = 20,000 ft, wing skew = 45°.

$A_p$

$$\begin{bmatrix} -0.7826 & 0.0958 & 0.0000 & 0.0030 & 0.9926 & -0.0003 \\ -0.0592 & -0.2908 & 0.0387 & 0.0259 & 0.0001 & -0.9920 \\ 0.0000 & 0.0000 & 0.0000 & 1.0000 & 0.0000 & 0.0275 \\ 33.1431 & -53.6928 & 0.0000 & -3.1250 & 2.0552 & 1.7210 \\ -8.6816 & 0.7975 & 0.0000 & 0.1679 & -1.0352 & 0.1810 \\ -1.0092 & 10.7521 & 0.0000 & -0.0213 & 0.0080 & -0.7129 \end{bmatrix}$$

$B_p$

$$\begin{bmatrix} -0.0974 & -0.0974 & -0.0198 & -0.0302 & 0.0000 \\ -0.0166 & 0.0166 & 0.0008 & -0.0005 & 0.0647 \\ 0.0000 & 0.0000 & 0.0000 & 0.0000 & 0.0000 \\ 12.9304 & -22.2654 & 15.8467 & -11.8422 & 13.2774 \\ -9.4073 & -10.8655 & -1.2311 & 0.8797 & 0.5694 \\ 1.9854 & -2.2579 & 0.5262 & -0.3276 & -6.2499 \end{bmatrix}$$

$H_p$

$$\begin{bmatrix} 0.0000 & 0.0000 & 0.0000 & 1.0000 & 0.0000 & 0.0000 \\ 0.0000 & 0.0000 & 0.0000 & 0.0000 & 1.0000 & 0.0000 \\ 0.0000 & 0.0000 & 0.0000 & 0.0000 & 0.0000 & 1.0000 \\ 0.0000 & 0.0000 & 1.0000 & 0.0000 & 0.0000 & 0.0000 \\ 20.1511 & -2.4782 & 0.0000 & 0.0302 & 0.1895 & 0.0097 \\ -1.5285 & -7.4982 & 0.0000 & -0.0426 & 0.0036 & 0.1972 \end{bmatrix}$$

$F_p$

$$\begin{bmatrix} 0.0000 & 0.0000 & 0.0000 & 0.0000 & 0.0000 \\ 0.0000 & 0.0000 & 0.0000 & 0.0000 & 0.0000 \\ 0.0000 & 0.0000 & 0.0000 & 0.0000 & 0.0000 \\ 0.0000 & 0.0000 & 0.0000 & 0.0000 & 0.0000 \\ 2.5097 & 2.5097 & 0.5103 & 0.7802 & -0.0033 \\ -0.4291 & 0.4291 & 0.0216 & -0.0120 & 1.6674 \end{bmatrix}$$

Table 2. Desired model system matrices.

$A_m$

$$\begin{bmatrix} -1.1568 & 0.0000 & 0.0000 & 0.0000 & 0.9566 & 0.0000 \\ 0.0000 & -0.2852 & 0.0387 & -0.0148 & 0.0000 & -0.9600 \\ 0.0000 & 0.0000 & 0.0000 & 1.0000 & 0.0000 & 0.0000 \\ 0.0000 & -41.7362 & 0.0000 & -8.0000 & 0.0000 & 10.0000 \\ -16.8252 & 0.0000 & 0.0000 & 0.0000 & -4.0271 & 0.0000 \\ 0.0000 & 10.9181 & 0.0000 & -0.2726 & 0.0000 & -3.3632 \end{bmatrix}$$

$B_m$

$$\begin{bmatrix} -0.0848 & -0.0848 & -0.0494 & -0.0494 & 0.0000 \\ -0.0166 & 0.0166 & 0.0000 & 0.0000 & 0.0647 \\ 0.0000 & 0.0000 & 0.0000 & 0.0000 & 0.0000 \\ 11.7086 & -11.7086 & 29.2528 & -29.2528 & 8.1349 \\ -7.8228 & -7.8228 & 0.0000 & 0.0000 & 0.0000 \\ 0.0000 & 0.0000 & 0.0000 & 0.0000 & -6.4014 \end{bmatrix}$$

$H_m$

$$\begin{bmatrix} 0.0000 & 0.0000 & 0.0000 & 1.0000 & 0.0000 & 0.0000 \\ 0.0000 & 0.0000 & 0.0000 & 0.0000 & 1.0000 & 0.0000 \\ 0.0000 & 0.0000 & 0.0000 & 0.0000 & 0.0000 & 1.0000 \\ 0.0000 & 0.0000 & 1.0000 & 0.0000 & 0.0000 & 0.0000 \\ 28.5286 & 0.0000 & 0.0000 & 0.0000 & 0.2342 & 0.0000 \\ 0.0000 & -7.3538 & 0.0000 & -0.0394 & 0.0000 & 0.2075 \end{bmatrix}$$

$F_m$

$$\begin{bmatrix} 0.0000 & 0.0000 & 0.0000 & 0.0000 & 0.0000 \\ 0.0000 & 0.0000 & 0.0000 & 0.0000 & 0.0000 \\ 0.0000 & 0.0000 & 0.0000 & 0.0000 & 0.0000 \\ 0.0000 & 0.0000 & 0.0000 & 0.0000 & 0.0000 \\ 2.1840 & 2.1840 & 1.2743 & 1.2743 & 0.0000 \\ -0.4291 & 0.4291 & 0.0000 & 0.0000 & 1.6674 \end{bmatrix}$$

Table 3. Closed-loop eigenvalues for full-state and output feedback.

Full-state feedback	Output feedback
$-7.4002 \pm 4.1541i$	$-7.1095 \pm 4.8533i$
$-6.1927 \pm 3.7359i$	$-5.3189 \pm 4.1278i$
$-3.5624 \pm 2.3180i$	$-3.3258 \pm 2.4188i$
-0.2347	-0.2271
-0.0341	-0.0317
-0.0011	-0.0011
Model eigenvalues	
$-2.5920 \pm 3.7464i$	Short period
$-3.5624 \pm 2.3180i$	Dutch-roll
-0.0120	Spiral
-7.9137	Roll

Table 4. Model feedforward, error feedback, and integral error feedback gain matrices flight condition;  
 $M = 0.8$ , altitude = 20,000 ft, wing skew = 45°.

$K_m$

$$\begin{bmatrix} -0.4449 & 0.1051 & 0.0006 & -0.0409 & 0.0485 & 0.0261 \\ 1.1031 & -0.3790 & 0.0017 & 0.0613 & 0.1025 & 0.0051 \\ -0.5542 & 0.2179 & -0.0001 & -0.0359 & -0.0234 & 0.0340 \\ 0.5025 & -0.1434 & -0.0021 & 0.0258 & 0.0164 & -0.0275 \\ -0.7614 & -0.5524 & 0.0012 & -0.0286 & -0.1194 & 0.1726 \end{bmatrix}$$

$K_p$

$$\begin{bmatrix} -0.1694 & 0.4585 & -0.1858 & -0.6725 & 0.0055 & -0.1032 \\ 0.2076 & 0.3803 & 0.1436 & 0.7338 & 0.0717 & 0.0521 \\ -0.1346 & 0.0891 & -0.0243 & -0.4903 & -0.0200 & -0.0760 \\ 0.0992 & -0.0900 & 0.0101 & 0.3344 & -0.0179 & 0.0476 \\ -0.1042 & 0.0085 & 0.5972 & -0.1658 & -0.0255 & -0.0145 \end{bmatrix}$$

$K_{Ie}$

$$\begin{bmatrix} -0.4697 & 0.7455 & -0.1821 \\ 0.5597 & 0.6492 & 0.1385 \\ -0.3838 & 0.1587 & -0.0805 \\ 0.3108 & -0.3873 & 0.0219 \\ -0.4845 & 0.2165 & 0.3367 \end{bmatrix}$$

## APPENDIX

The following informal proof shows that the projection from state space to output space preserves the augmented system closed-loop eigenvalues if the number of unique outputs is greater than or equal to the number of states.

Given the system equations

$$\dot{\mathbf{x}} = \mathbf{A}\mathbf{x} + \mathbf{B}\mathbf{u} \quad (21)$$

$$\mathbf{y} = \mathbf{H}\mathbf{x} + \mathbf{F}\mathbf{u} \quad (22)$$

Where  $(\mathbf{A}, \mathbf{B})$  is stabilizable,  $(\mathbf{H}, \mathbf{A})$  is observable,  $\mathbf{H}$  is full rank, and  $\text{Rank}(\mathbf{H}) \geq \text{Rank}(\mathbf{A})$ .

Given the optimal control in the form  $\mathbf{u} = -\mathbf{K}_x\mathbf{x}$ . Then the closed-loop system equation becomes the following

$$\dot{\mathbf{x}} = (\mathbf{A} - \mathbf{B}\mathbf{K}_x)\mathbf{x} \quad (23)$$

To determine the output form of the control, premultiply the output equation by  $(\mathbf{H}^T\mathbf{H})^{-1}\mathbf{H}^T$  to get

$$(\mathbf{H}^T\mathbf{H})^{-1}\mathbf{H}^T\mathbf{y} = \mathbf{x} + (\mathbf{H}^T\mathbf{H})^{-1}\mathbf{H}^T\mathbf{F}\mathbf{u} \quad (24)$$

This inverse exists since  $\mathbf{H}$  is full rank (by assumption). Substituting into the optimal control equation yields

$$\mathbf{u} = -\mathbf{K}_x(\mathbf{H}^T\mathbf{H})^{-1}\mathbf{H}^T\mathbf{y} + \mathbf{K}_x(\mathbf{H}^T\mathbf{H})^{-1}\mathbf{H}^T\mathbf{F}\mathbf{u} \quad (25)$$

which can be rewritten in the final output form

$$\mathbf{u} = -\underbrace{[\mathbf{I} - \mathbf{K}_x(\mathbf{H}^T\mathbf{H})^{-1}\mathbf{H}^T\mathbf{F}]^{-1}\mathbf{K}_x(\mathbf{H}^T\mathbf{H})^{-1}\mathbf{H}^T}_{\mathbf{K}_y}\mathbf{y} \quad (26)$$

To examine the closed-loop eigenvalues of the output feedback system, substitute equation (26) into the system equations to yield

$$\dot{\mathbf{x}} = \mathbf{A}\mathbf{x} - \mathbf{B}\mathbf{K}_y\mathbf{y} \quad (27)$$

$$\mathbf{y} = \mathbf{H}\mathbf{x} - \mathbf{F}\mathbf{K}_y\mathbf{y} \quad (28)$$

Rewriting this last equation

$$\mathbf{y} = [\mathbf{I} + \mathbf{F}\mathbf{K}_y]^{-1}\mathbf{H}\mathbf{x} \quad (29)$$

Thus the closed-loop output feedback system equation becomes

$$\dot{\mathbf{x}} = (\mathbf{A} - \mathbf{B}\mathbf{K}_y[\mathbf{I} + \mathbf{F}\mathbf{K}_y]^{-1}\mathbf{H})\mathbf{x} \quad (30)$$

To show that the closed-loop eigenvalues of the state feedback (eq. 23) and output feedback (eq. 30) systems are the same, it is sufficient to show that the closed-loop dynamic equations of the two systems are identical. Comparing the two equations, it is necessary to show that  $\mathbf{K}_x = \mathbf{K}_y[\mathbf{I} + \mathbf{F}\mathbf{K}_y]^{-1}\mathbf{H}$ .

From the definition of  $\mathbf{K}_y$  (eq. 26),

$$[\mathbf{I} - \mathbf{K}_x(\mathbf{H}^T\mathbf{H})^{-1}\mathbf{H}^T\mathbf{F}]\mathbf{K}_y = \mathbf{K}_x(\mathbf{H}^T\mathbf{H})^{-1}\mathbf{H}^T \quad (31)$$

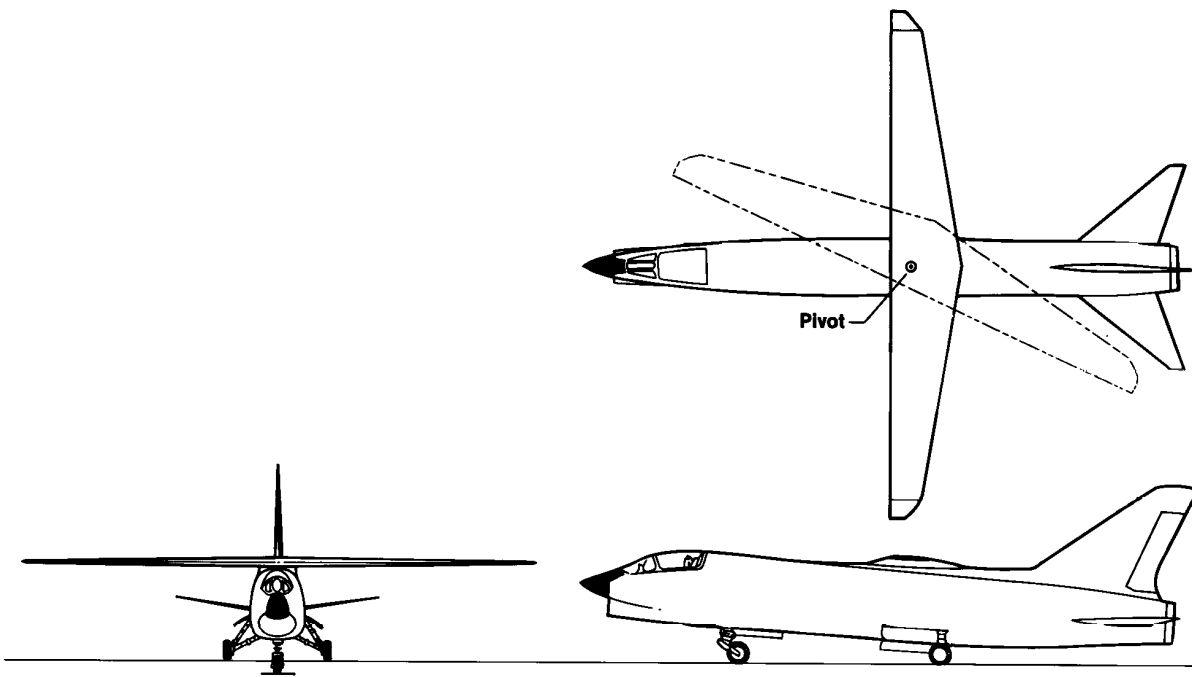
$$K_y = K_x(H^T H)^{-1} H^T [I + FK_y] \quad (32)$$

Collecting  $K_y$  terms and post multiplying by  $H$  results in,

$$K_x = K_y[I + FK_y]^{-1} H \quad (33)$$

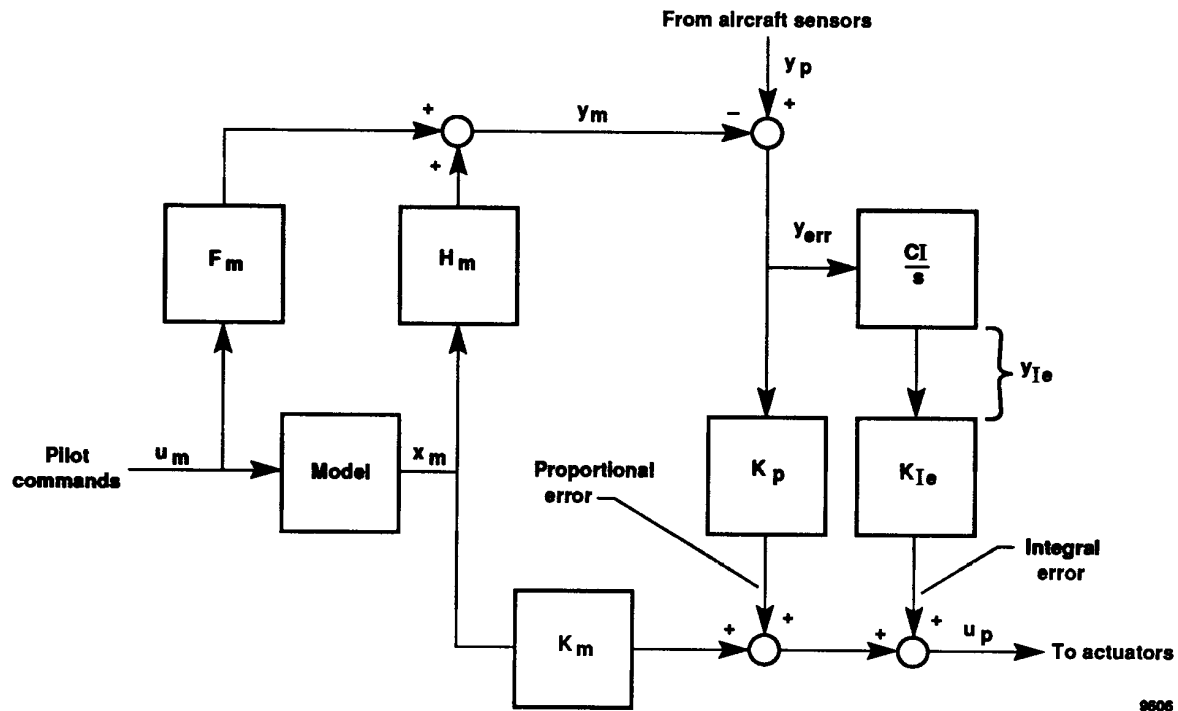
## REFERENCES

- Alag, G.S., R.W. Kempel, J.W. Pahle, J.J. Bresina, and F. Bartoli, *Model Following Control for an Oblique-Wing Aircraft*, NASA TM-88269, 1986.
- Bryson, A.E., and Y.C. Ho, *Applied Optimal Control*, Revised Edition, Hemisphere Publishing Corporation, 1975.
- Duke, E.L., B.P. Patterson, and R.F. Antoniewicz, *User's Manual for LINEAR, a FORTRAN Program to Derive Linear Aircraft Models*, NASA TP-2768, 1987.
- Graham, A., R.T. Jones, J. Summers, *Wind Tunnel Test of an F-8 Airplane Model Equipped with an Oblique Wing*, NASA TM X-62273, 1973.
- Gregory, T., "Oblique Wing Ready for Research Aircraft," *Aerospace America*, June 1985, pp. 78-81.
- McMurtry, T.C., A.G. Sim, and W.H. Andrews, "AD-1 Oblique Wing Aircraft Program," AIAA-81-2354, Nov. 1981.
- Nelms, W.P., Jr., "Applications of Oblique Wing Technology - An Overview," AIAA-76-943, Sept. 1976.
- Smith, R., R.T. Jones, and J. Summers, *Transonic Wind Tunnel Tests of an F-8 Airplane Model Equipped with 12 and 14-percent Thick Oblique Wings*, NASA TM X-62478, 1975.
- Smith, R., R.T. Jones, and J. Summers, *Transonic Longitudinal and Lateral Control Characteristics of an F-8 Airplane Model Equipped with an Oblique Wing*, NASA TM X-73103, 1976.
- Tyler, J.S., Jr., "The Characteristics of Model Following Systems as Synthesized by Optimal Control," *IEEE Transactions on Automatic Control*, Oct. 1964.
- Vincent, J.H., "Direct Incorporation of Flying Qualities Criteria Into Multivariate Flight Control Design," AIAA-84-1830-CP, Aug. 1984.
- White, S., et al., *A Feasibility Design Study for an F-8 Oblique Wing Research Demonstrator*, Final Report, NASA CR NAS-11409, 1984.
- Wiler, C.D., and S.N. White, "Projected Advantage of an Oblique Wing Design on a Fleet Air Defense Mission," *J. Aircraft*, Vol. 22, No. 10, Oct. 1985, pp. 896-900.



8311

Figure 1. Three view of proposed OWRA configuration.



9806

Figure 2. Closed-loop control system block diagram of explicit model following.

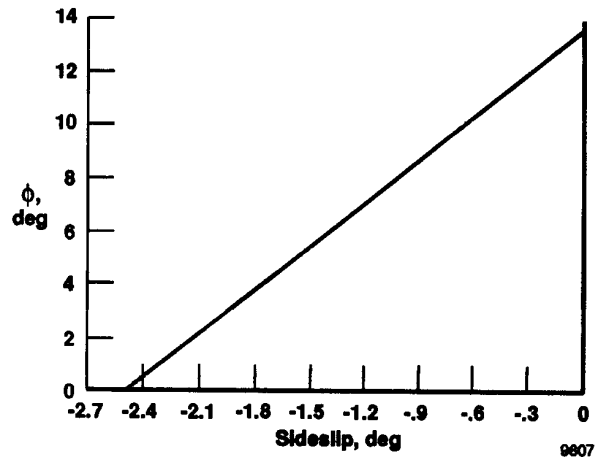


Figure 3. Trim sideslip as a function of roll angle flight condition;  $M = 0.8$ , altitude = 20,000 ft, wing skew =  $65^\circ$ .

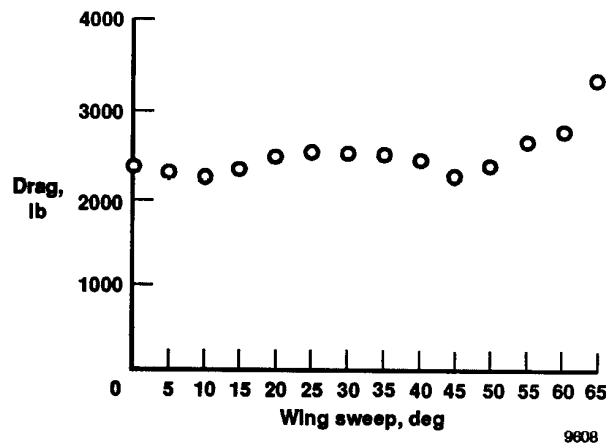


Figure 4. Total aircraft drag as a function of wing skew flight condition;  $M = 0.8$ , altitude = 20,000 ft, sideslip trim.

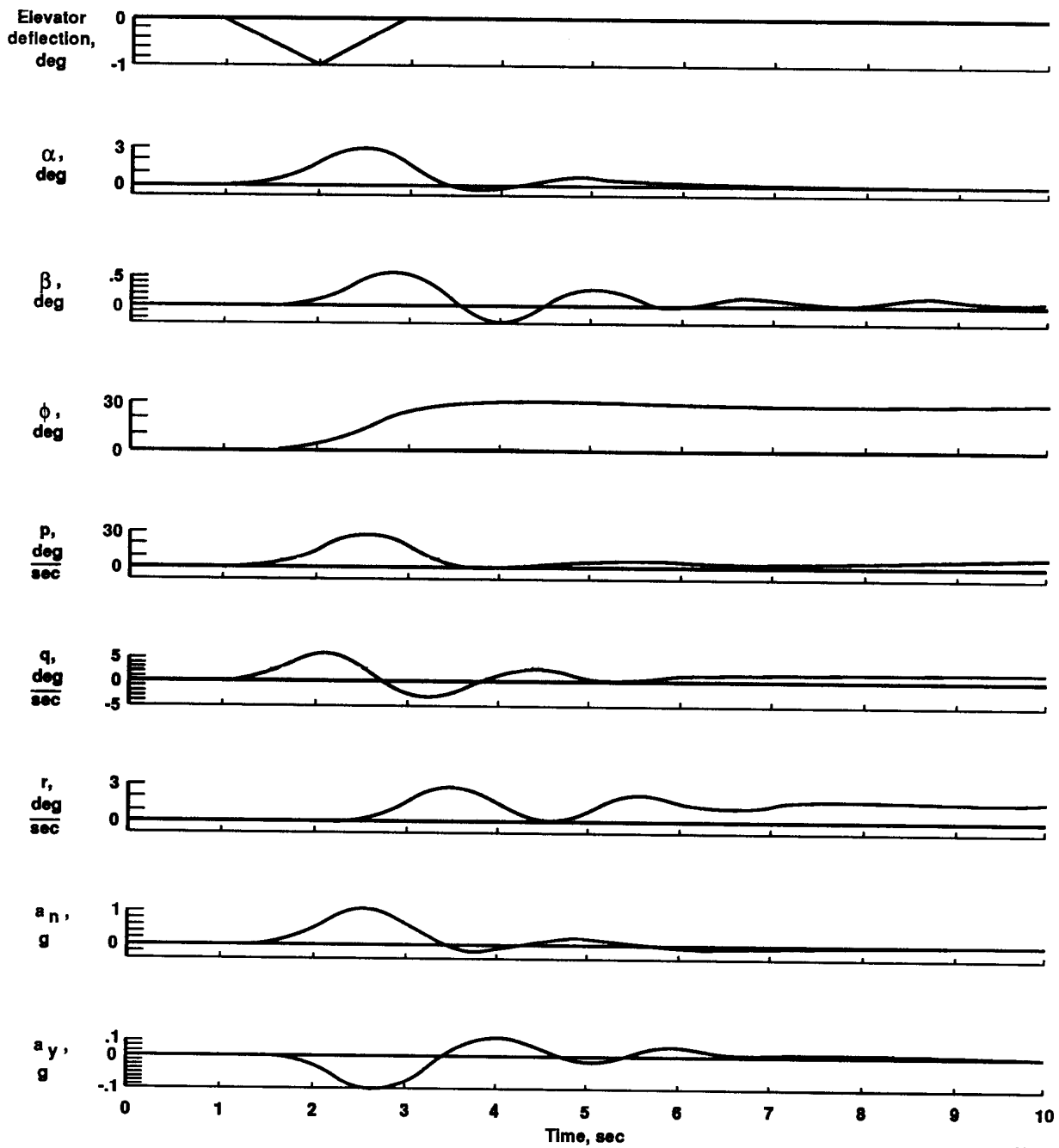


Figure 5. Open-loop aircraft response to 1°-pitch ramp.

9609

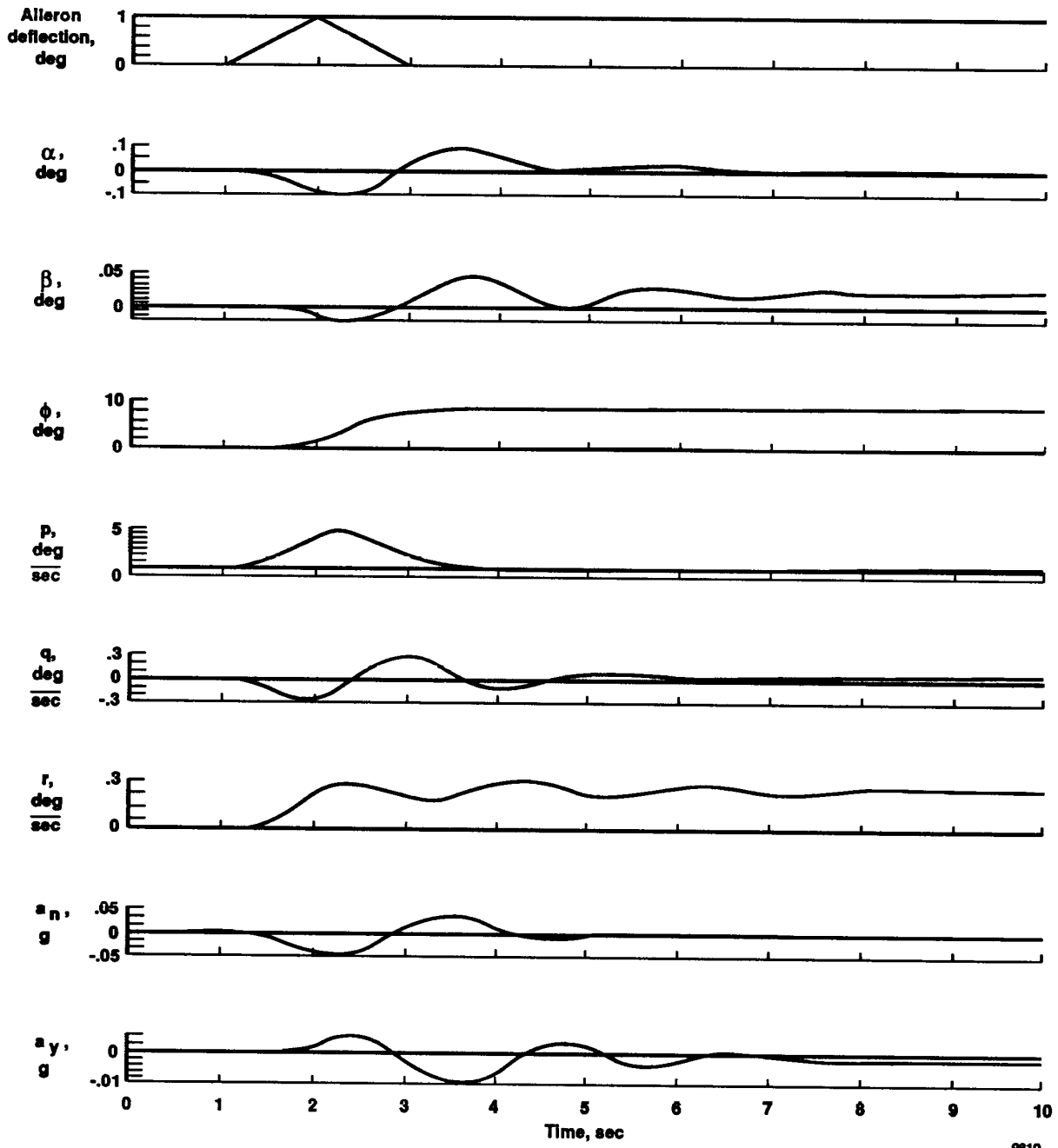


Figure 6. Open-loop aircraft response to 1°-roll ramp.

9610

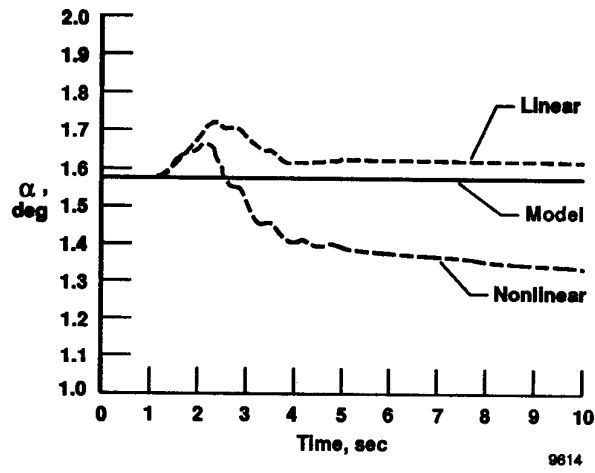


Figure 7. Closed-loop aircraft response to roll ramp angle of attack.

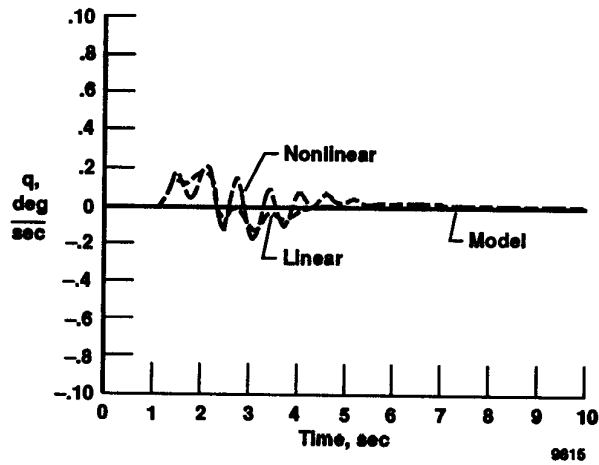


Figure 8. Closed-loop aircraft response to roll ramp pitch rate.

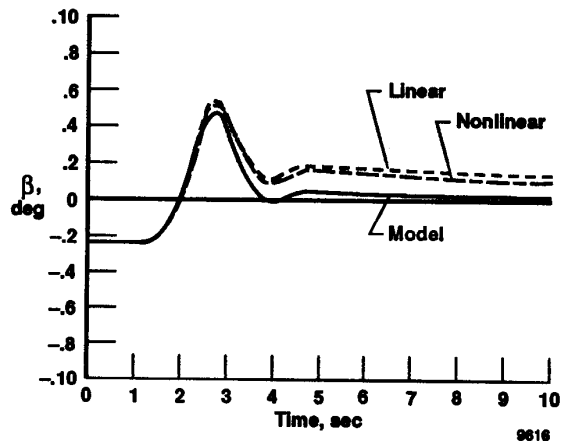


Figure 9. Closed-loop aircraft response to roll ramp sideslip angle.

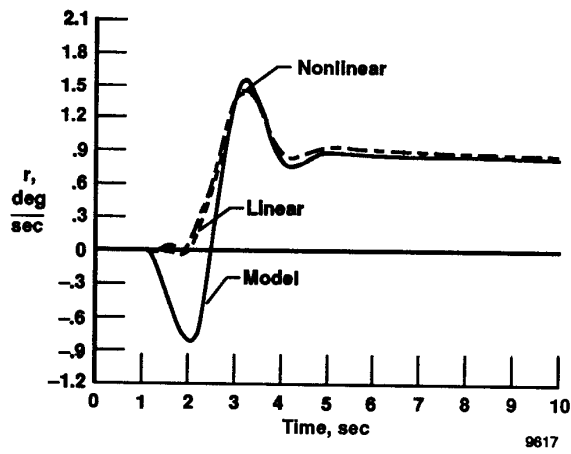


Figure 10. Closed-loop aircraft response to roll ramp yaw rate.

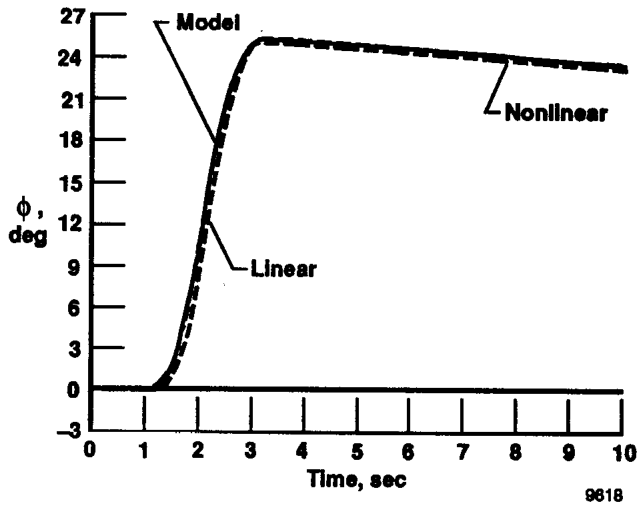


Figure 11. Closed-loop aircraft response to roll ramp roll angle.

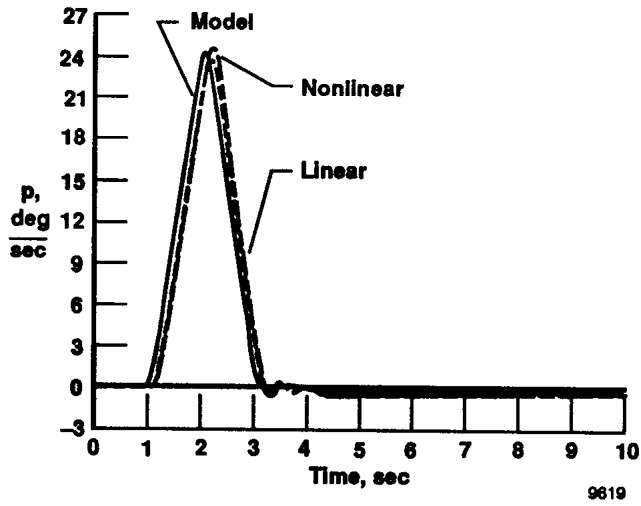


Figure 12. Closed-loop aircraft response to roll ramp roll rate.

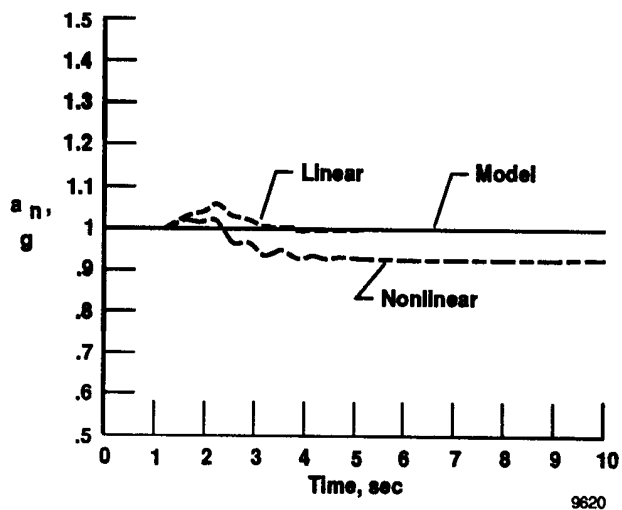


Figure 13. Closed-loop aircraft response to roll ramp normal acceleration.

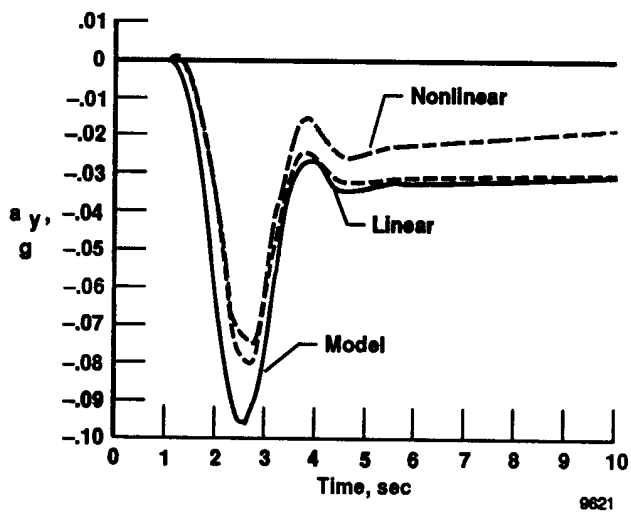


Figure 14. Closed-loop aircraft response to roll ramp lateral acceleration.

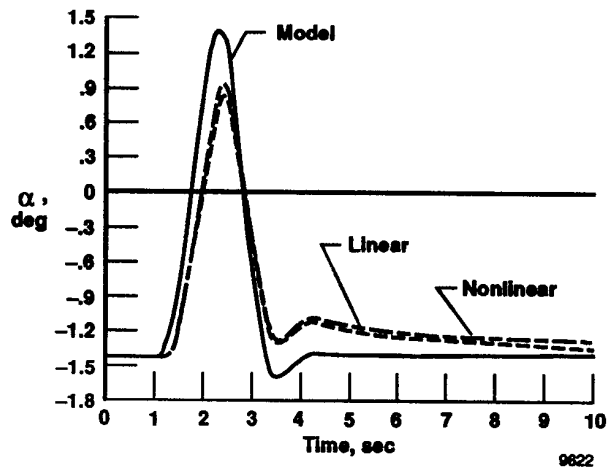


Figure 15. Closed-loop aircraft response to pitch ramp angle of attack.

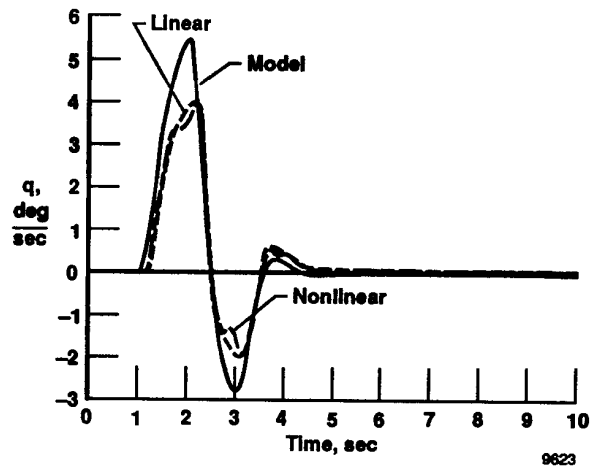


Figure 16. Closed-loop aircraft response to pitch ramp pitch rate.

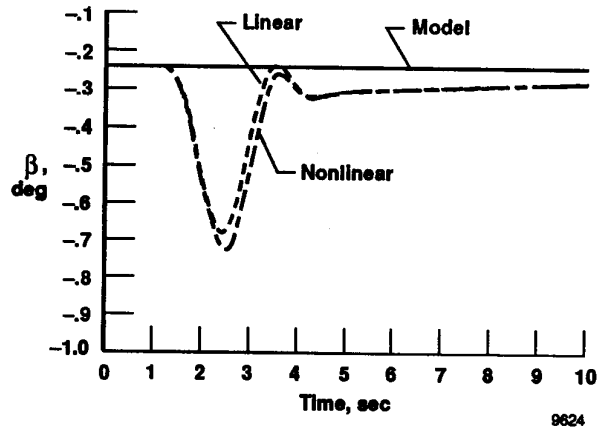


Figure 17. Closed-loop aircraft response to pitch ramp sideslip angle.

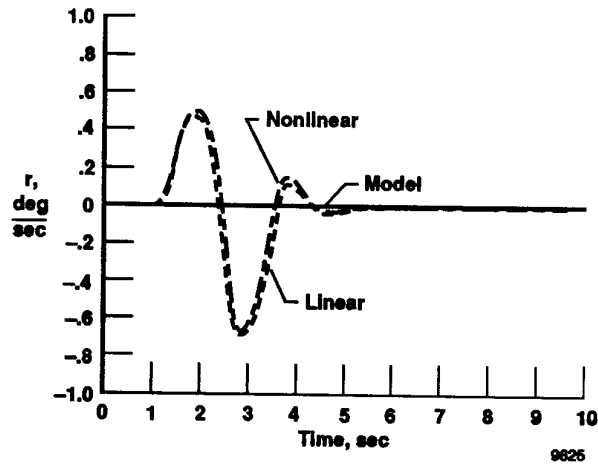


Figure 18. Closed-loop aircraft response to pitch ramp yaw rate.

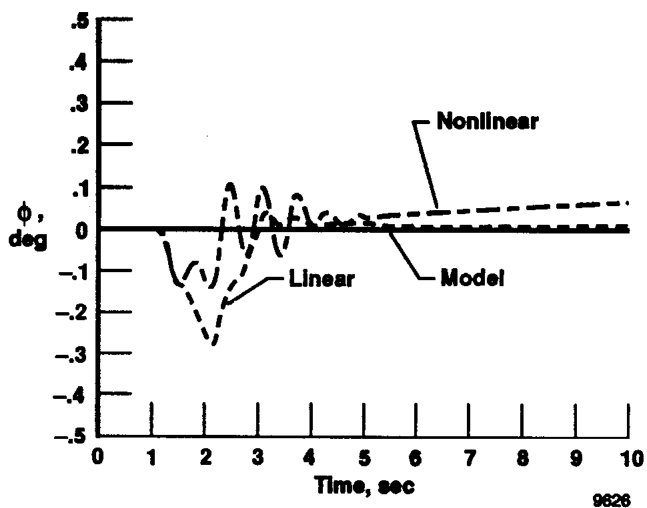


Figure 19. Closed-loop aircraft response to pitch ramp roll angle.

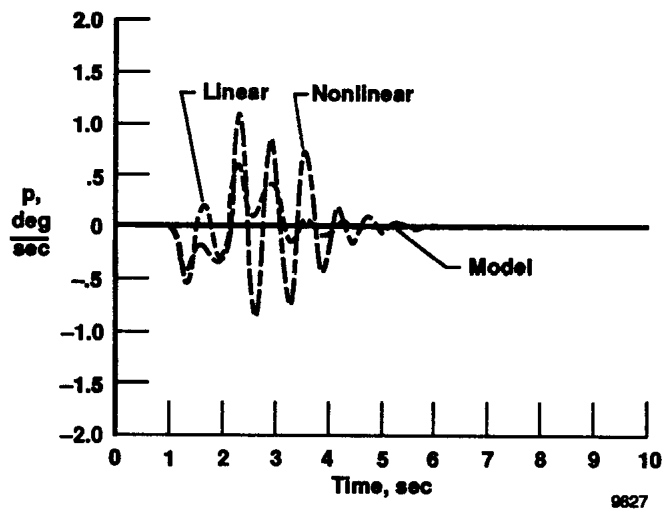


Figure 20. Closed-loop aircraft response to pitch ramp roll rate.

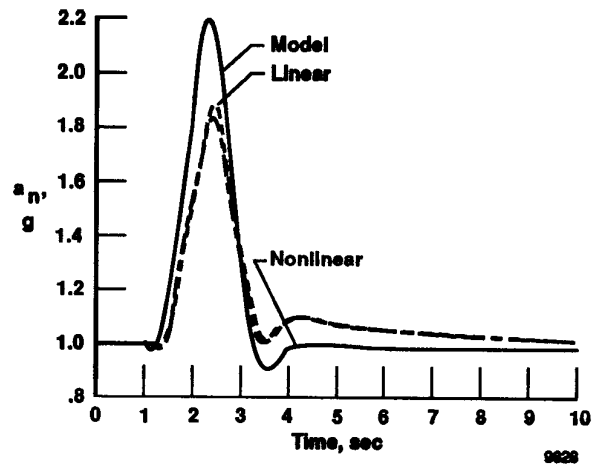


Figure 21. Closed-loop aircraft response to pitch ramp normal acceleration.

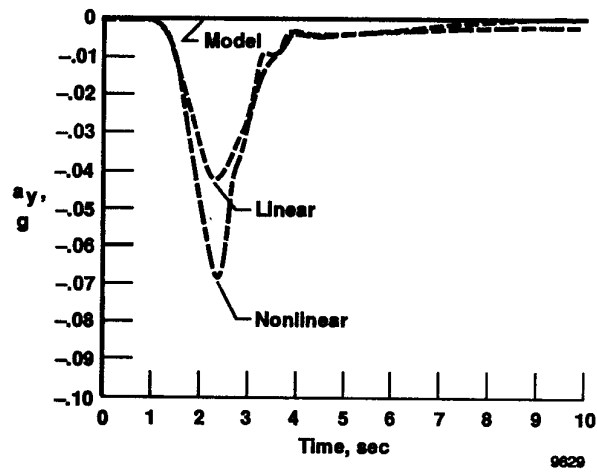


Figure 22. Closed-loop aircraft response to pitch ramp lateral acceleration.



# Report Documentation Page

1. Report No. <b>NASA TM-100454</b>		2. Government Accession No.		3. Recipient's Catalog No.	
4. Title and Subtitle <b>Output Model-Following Control Synthesis for an Oblique-Wing Aircraft</b>				5. Report Date <b>April 1990</b>	
				6. Performing Organization Code	
7. Author(s) <b>Joseph W. Pahle</b>				8. Performing Organization Report No. <b>H-1522</b>	
				10. Work Unit No. <b>RTOP 533-06-01</b>	
9. Performing Organization Name and Address <b>NASA Ames Research Center Dryden Flight Research Facility P.O. Box 273, Edwards, CA 93523-0273</b>				11. Contract or Grant No.	
				13. Type of Report and Period Covered <b>Technical Memorandum</b>	
12. Sponsoring Agency Name and Address <b>National Aeronautics and Space Administration Washington, DC 20546</b>				14. Sponsoring Agency Code	
				15. Supplementary Notes	
16. Abstract <p>Recent interest in oblique-wing aircraft has focused on the potential aerodynamic performance advantage of a variable-skew oblique wing over a conventional or symmetric sweep wing. Unfortunately, the resulting asymmetric configuration has significant aerodynamic and inertial cross-coupling between the aircraft longitudinal and lateral-directional axes. This paper presents a decoupling control law synthesis technique that integrates stability augmentation, decoupling, and the direct incorporation of desired handling qualities into an output feedback controller. The proposed design technique uses linear quadratic regulator concepts in the framework of explicit model following. The output feedback strategy used is a suboptimal projection from the state space to the output space. Dynamics are then introduced into the controller to improve steady-state performance and increase system robustness. Closed-loop performance is shown by application of the control laws to the linearized equations of motion and nonlinear simulation of an oblique-wing aircraft.</p>					
17. Key Words (Suggested by Author(s)) <b>Automatic control Control law synthesis Model-following Oblique wing</b>			18. Distribution Statement <b>Unclassified — Unlimited</b>  <b>Subject category 08</b>		
19. Security Classif. (of this report) <b>Unclassified</b>		20. Security Classif. (of this page) <b>Unclassified</b>		21. No. of pages <b>29</b>	22. Price <b>A03</b>